

Vacuum-Assisted Strong Luminescence Thermal Enhancement in NaYF₄:Ho³⁺/Yb³⁺ Upconverting Nanocrystals: A Conclusive Evidence for the Effect of Water Desorption

Lin Yang, Hao Wu, Guo-hui Pan, Liangliang Zhang, Huajun Wu, Zhendong Hao, Feng Liu,* and Jiahua Zhang*



Cite This: *ACS Sustainable Chem. Eng.* 2022, 10, 16862–16870



Read Online

ACCESS |



Metrics & More



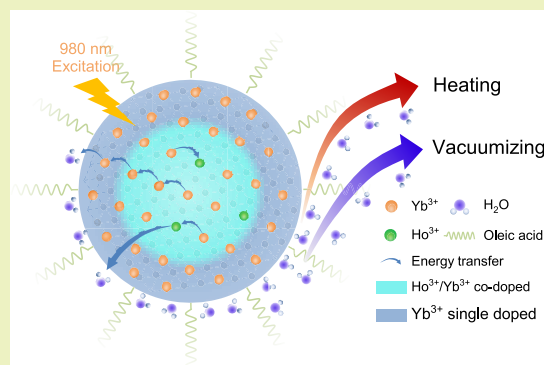
Article Recommendations



Supporting Information

ABSTRACT: The luminescence thermal enhancement (LTE), in lanthanide-doped upconverting nanocrystals (UCNCs), has attracted extensive attention for its applications in anticounterfeiting, temperature sensing, and so on. Some mechanisms for LTE were proposed, including thermally induced water desorption from the surface of UCNCs, but conclusive evidence is absent for any of the mechanisms. Here, vacuumizing is employed in the experiment for the LTE in NaYF₄:Ho³⁺/Yb³⁺ UCNCs, and significantly promoted LTE is observed. The 300–450–300 K temperature cycling experiment in vacuum shows continuous luminescence enhancement without luminescence intensity recovery as in the cooling process in moisture air, indicating the effect of water desorption because water readsorption is blocked in vacuum. It is found that the Ho³⁺ ⁵I₆ level can be deexcited by direct long-range energy transfer to water adsorbed at the surface of nanocrystals due to resonant coupling between the Ho³⁺ ⁵I₆ → ⁵I₇ transition and the –OH vibration of water. As a result, water desorption suppresses the ⁵I₆ depopulation and thus enhances the luminescence of Ho³⁺. Finally, the regulation of upconversion LTE is realized by adjusting the size of nanocrystals and Ho³⁺ or Yb³⁺ concentrations. Our findings indicate that the vacuumizing technique is an effective method to distinguish water-desorption-induced LTE. This work deepens the understanding of LTE and offers insights into the regulation of LTE.

KEYWORDS: upconversion luminescence, thermal enhancement of luminescence, nanocrystals, NaYF₄:Ho³⁺, Yb³⁺, FRET, core–shell structure



INTRODUCTION

Energy transfer upconversion (ETU) of Yb³⁺ and Ln³⁺ (Ln³⁺ = Er³⁺, Tm³⁺, Ho³⁺) codoped upconverting phosphors has been extensively studied for their unique nonlinear optical properties.^{1–9} In 2014, Shao et al.¹⁰ reported thermally enhanced upconversion luminescence (UCL) in Er³⁺/Yb³⁺ codoped upconverting nanocrystals (UCNCs). Since then, the luminescence thermal enhancement (LTE) in lanthanide-doped UCNCs has received considerable attention due to its potential applications in anticounterfeiting, temperature sensing, thermochromism display technology, and so on.^{11–15} There are several mechanisms proposed for LTE.^{16–18} Yb–O surface phonons are considered to be responsible for LTE in NaYF₄:Yb,Tm nanocrystals (NCs) through activating the surface dark-layer by enhancing energy transfer from Yb³⁺.^{19,20} An interesting mechanism was employed for LTE of NaY(WO₄)₂,²¹ namely, thermal desorption of water from the NC surface.^{22–24} This mechanism is supported by the observation of LTE suppression for NCs in dry nitrogen. In addition, it was found that LTE is absent in bulk NaY(WO₄)₂,

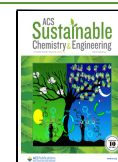
implying that LTE is not related to the Yb–O vibration. Cheng et al. proposed another mechanism, namely, thermally induced lattice expansion. This process deactivates the energy migration from the NC interior to the surface to suppress the surface-related quenching effect.^{25,26} However, the confirmations of these possible mechanisms still need conclusive evidence. Here, we propose a method for verifying water-desorption-induced LTE.

With consideration that water desorption can be forced to occur under negative pressure,²⁷ we propose a method, namely, vacuum-assisted LTE. It is expected that the vacuum environment will promote LTE if water desorption dominates the LTE. Moreover, the vacuum environment will still keep the

Received: September 9, 2022

Revised: November 20, 2022

Published: December 8, 2022



enhanced luminescence in the cooling process because readsorption of water is blocked in vacuum. Hence, the method of vacuum-assisted LTE could test the role of water desorption and deepen the understanding of water desorption processes.

The origin of water-desorption-induced LTE is actually the suppression of luminescence quenching caused by water. The quenching pathway is generally considered to be the consequence of depletion of excited sensitizer Yb^{3+} ions due to energy migration from Yb^{3+} in the core to Yb^{3+} at the surface, where the energy is dissipated by the adsorbed water.^{28–30} Generally, luminescence quenching caused by the surface-adsorbed water of NCs can be effectively suppressed by coating an inert shell with the thickness of several nanometers;^{31–35} for instance, the upconversion LTE in $\text{Yb}^{3+}/\text{Tm}^{3+}$ codoped NaYF_4 UCNCs disappears after a 3.5 nm-thick shell coating.²¹ However, the upconversion LTE can still be observed in $\text{Yb}^{3+}/\text{Er}^{3+}$ codoped NaYF_4 UCNCs coated with a 10 nm-thick shell,³⁶ implying a long quenching range of Er^{3+} . Even though, in truth, the interaction between the interior activator and external quenchers, such as solvent molecules, has been studied,^{37,38} its contribution to LTE has not been paid enough attention in previous studies. In addition, there have been relatively few studies on the LTE of the $\text{Yb}^{3+}/\text{Ho}^{3+}$ system because the application potential of the $\text{Yb}^{3+}/\text{Ho}^{3+}$ system is less than that of the $\text{Yb}^{3+}/\text{Er}^{3+}$ system and the $\text{Yb}^{3+}/\text{Tm}^{3+}$ system. However, the $\text{Yb}^{3+}/\text{Ho}^{3+}$ system is very suitable for studying the mechanism of LTE because the emissions of upconversion intermediate levels of Ho^{3+} ($^5\text{I}_6$ state) and Yb^{3+} ($^2\text{F}_{5/2}$ state) are separated from each other, which can accurately determine the changes in the activator and sensitizer during the heating process.

In this paper, vacuumizing is employed to verify the role of water desorption on LTE in $\text{Ho}^{3+}/\text{Yb}^{3+}$ doped NCs. Vacuum-assisted strong thermal enhancement of UCL is observed in $\text{Ho}^{3+}/\text{Yb}^{3+}$ codoped nanocrystals. It is found that the $\text{Ho}^{3+} ^5\text{I}_6$ level can be deexcited by direct long-range energy transfer to water adsorbed at the surface of NCs due to resonant coupling between $\text{Ho}^{3+} ^5\text{I}_6 \rightarrow ^5\text{I}_7$ transition and the $-\text{OH}$ vibration of water. The water desorption suppresses the deexcitation of Ho^{3+} and enhances UCL. The regulation of luminescence enhancement is realized by designing core-shell structures with variable sizes and doping concentrations.

EXPERIMENTAL SECTION

Chemicals. NH_4F (>96%), NaOH (>96%), and HCl were supplied from Beijing Chemical Reagent Company. Hexanes, ethanol, and methanol were obtained from XiLong Scientific. Ln_2O_3 ($\text{Ln} = \text{Y}, \text{Yb}, \text{Ho}$, >99.99%) were purchased from the Yangjiang rare earth company. Oleic acid (OA, 90%) and 1-octadecene (ODE, 90%) were purchased from Sigma-Aldrich. Oleylamine (OM, 80–90%) was purchased from Aladdin. $\text{LnCl}_3 \cdot 6\text{H}_2\text{O}$ ($\text{Ln} = \text{Y}, \text{Yb}, \text{Ho}$) was prepared by dissolving the corresponding lanthanide oxides in hydrochloric acid.

Synthesis of $\beta\text{-NaYF}_4$ Core NCs. $\beta\text{-NaYF}_4\text{:Ln}$ ($\text{Ln} = \text{Yb}$ or Ho) core NCs were synthesized following a reported approach.³⁹ In a typical synthesis, 1 mmol of $\text{LnCl}_3 \cdot 6\text{H}_2\text{O}$ ($\text{Ln} = \text{Y}, \text{Yb}, \text{Ho}$), 6 mL of OA, and 15 mL of ODE were mixed in a 100 mL three-necked flask. The mixture was heated to 140 °C under magnetic stirring and a flow of N_2 for 30 min to form a transparent solution and then cooled down to 50 °C. Subsequently, 2.5 mL of a NaOH methanol solution (1 M) and 10 mL of a NH_4F methanol solution (0.4 M) were quickly mixed and added into the flask and the reaction temperature was maintained at 50 °C for 30 min. After that, the mixed solution was heated slowly to 70 °C for 30 min to remove the methanol. The temperature was

then increased to 300 °C under a nitrogen atmosphere for 90 min while stirring. After naturally cooling down to room temperature, the synthetic NCs were washed several times by precipitation with the addition of ethanol, collection by centrifugation, and redispersion in cyclohexane. The final solid-state products were obtained after centrifugation and drying in an oven at 60 °C for 24 h.

Synthesis of the Shell Precursor. The $\alpha\text{-NaYF}_4\text{:Ln}$ ($\text{Ln} = \text{Y}, \text{Yb}$ or Ho) were synthesized as sacrificial shell precursors following a reported method,⁴⁰ where 6 mL of OA, 6 mL of OM, and 10 mL of ODE were placed into a three-necked flask together with 2 mmol of CF_3COONa and 2 mmol of $(\text{CF}_3\text{COO})_3\text{Ln}$ ($\text{Ln} = \text{Y}, \text{Yb}, \text{Ho}$). To dissolve the solid reagents and remove the residual water, the solution was magnetically stirred and heated to 120 °C for 30 min under a flow of N_2 until it became clear. The solution was then heated to 290 °C and allowed to react for 45 min in a N_2 atmosphere. Subsequently, the solution was cooled down to room temperature and the products were precipitated and washed with the addition of ethanol, collected by centrifugation, and finally dispersed in 8 mL of ODE for later use.

Synthesis of $\beta\text{-Core-Shell NCs}$. The homogeneous core-shell $\beta\text{-NaYF}_4$ NCs were synthesized following a reported approach.³⁶ First, 0.5 mmol of core $\beta\text{-NaYF}_4$ NCs was synthesized by the methods described above. Near the end of the synthetic reaction of the core sample, instead of being cooled down, 1 mL of the ODE solution of the dispersing prepared shell precursor was rapidly injected into the reaction solution by a syringe with a stainless steel cannula; meanwhile, the reaction conditions, including magnetic stirring, a N_2 atmosphere, and a reaction temperature at 300 K, were maintained for 15 min for epitaxial growth. The thermal injection and ripening process could be performed multiple times to increase the thickness of the epitaxial shell. Furthermore, the shell thickness could also be modulated by the amount of shell precursor in each injection. After the ripening, the solution was cooled down to room temperature. The synthetic NCs were washed several times by precipitation with the addition of ethanol, collection by centrifugation, and redispersion in cyclohexane. The final solid-state products were obtained after centrifugation and drying in an oven at 60 °C for 24 h.

Characterizations. The morphology was investigated by field emission scanning electron microscopy (SEM) (Hitachi S-4800). The spectra were measured using an FLS920 spectrometer (Edinburgh Instruments, U.K.), a QEPPro fiber spectrometer (200–1000 nm, Ocean Optics), and a NIRQUEST fiber spectrometer (900–2400 nm, Ocean Optics) pumped with a power-controllable 980 nm laser diode (LD) or a power-controllable 455 nm LD. The laser spot area is about 12.6 mm², and the laser power is about 70 mW in spectrum measurement, leading to a power density of 5.6 mW/mm². The relative humidity of the air during the spectral measurement is about 50%. The vacuum environment in the experiment is pumped by a mechanical pump with a vacuum level of 10^{−3} Torr. In the measurement of fluorescence decay, the wavelength-tunable pulse laser with 10 ns duration of a Surelite II-10 pumped Horizon OPO was used as the excitation source; the signal was detected using an R9110 PMT TCSPC (Hamamatsu, Japan) and recorded by a TDS3052B oscilloscope. All of the values of the calculated luminescence lifetime were the average lifetime in this work. A THMS600E cooling-heating platform (77–873 K, Linkam Scientific Instruments, U.K.) was used for offering different temperatures in temperature-dependent luminescence spectra and lifetime measurements in air. The vacuum heating platform was built as schematically shown in Figure S1.

RESULTS AND DISCUSSION

The upconversion LTE was observed in $\text{NaYF}_4\text{:2%Ho/20%Yb@NaYF}_4\text{:40%Yb}$ core-shell UCNCs, of which the hexagonal $\text{NaYF}_4\text{:2%Ho/20%Yb}$ core was synthesized via a coprecipitation method, and the $\text{NaYF}_4\text{:40%Yb}$ shell was coated on the core via the layer-by-layer epitaxial growth method. The SEM photographs show that the NaYF_4 cores before coating the shell are monodispersed with an average size of 33.8 ± 1.7 nm (Figure 1a,b). The core-shell UCNCs show

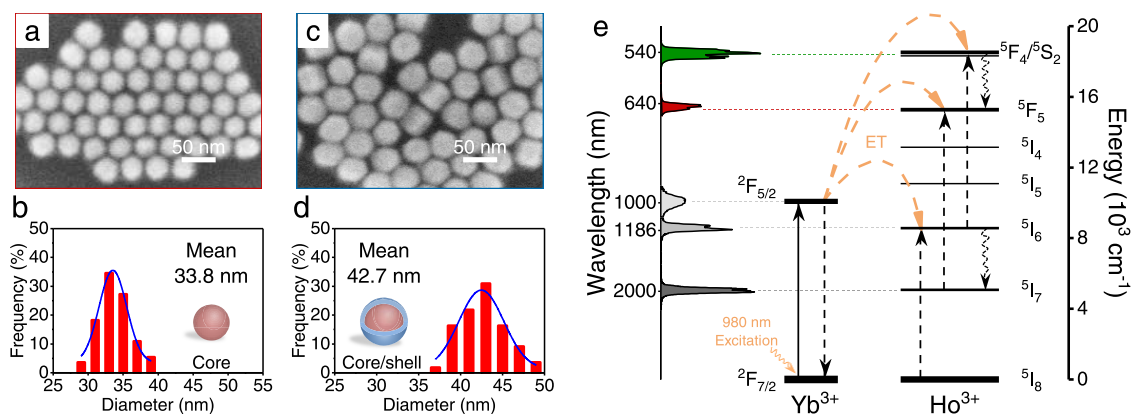


Figure 1. SEM images (a, c) and size distribution (b, d) of NaYF₄:2%Ho, 20%Yb core only, and NaYF₄:2%Ho, 20%Yb@NaYF₄:40%Yb core-shell UCNCs. (e) Ho³⁺ and Yb³⁺ energy-level diagrams as well as population processes and emission spectra of each energy level under 980 nm LD excitation.

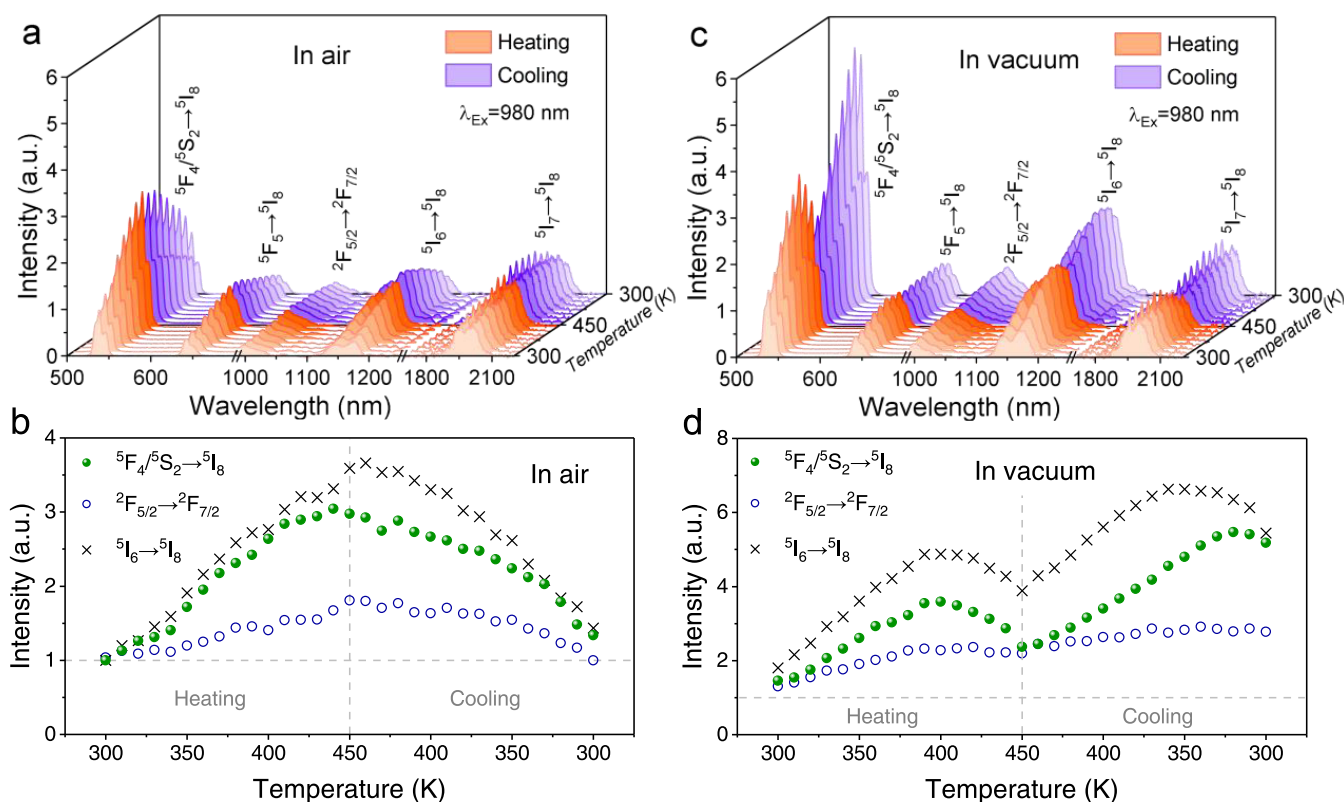


Figure 2. Temperature cycling experiment for thermally enhanced UCL in NaYF₄:2%Ho, 20%Yb@NaYF₄:40%Yb NCs under 980 nm LD excitation. (a, b) Temperature-dependent luminescence spectra and intensities of various emissions in air and (c, d) in vacuum. The intensities of various emissions in air at 300 K are normalized.

an average size of 42.7 ± 2.3 nm (Figure 1c, d). It is well known that the Ho–Yb upconverting system is a typical ETU system with Ho³⁺ as an emitter and Yb³⁺ as a sensitizer. The typical emission spectrum of core–shell UCNCs and the corresponding energy-level population process under 980 nm LD excitation are depicted in Figure 1e. It can be seen that there are five emission peaks in the spectrum. The green peak at 540 nm and the red one at 640 nm are upconversion emissions, originated from $^5S_2/^5F_4 \rightarrow ^5I_8$ and $^5F_5 \rightarrow ^5I_8$ transitions of Ho³⁺, respectively. The rest of the three peaks come from downshifting emissions. They are assigned to the $^2F_{5/2} \rightarrow ^2F_{7/2}$ transition of Yb³⁺ for the peak at 1000 nm as well as the $^5I_6 \rightarrow ^5I_8$ and $^5I_7 \rightarrow ^5I_8$ transitions of Ho³⁺ for the peaks

at 1186 nm and 2000 nm, respectively. Both the green and red upconversion emissions are two photon processes, i.e., excited by a two-step energy transfer from Yb³⁺. They share the first step energy transfer for populating the 5I_6 level. The $^5I_6 \rightarrow ^5S_2/^5F_4$ upward transition by the second step energy transfer populates the green $^5S_2/^5F_4$ level. The 5I_6 level may also relax nonradiatively down to the 5I_7 level, from which the red 5F_5 level can be populated by the second step energy transfer.

The temperature-dependent emission spectra of the core–shell UCNCs in the heating–cooling experiment (300–450 K) are measured in air and in vacuum, as shown in Figure 2a and 2c, respectively. It can be seen that all emissions exhibit thermal enhancement in the heating process either in air or in

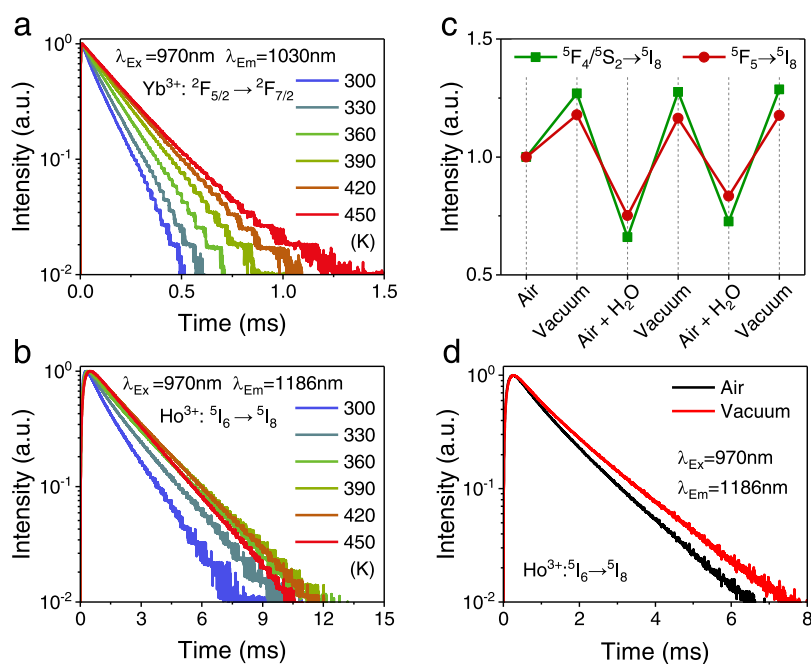


Figure 3. Emission decay curves of (a) ${}^2F_{5/2} \rightarrow {}^2F_{7/2}$ of Yb^{3+} and (b) ${}^5I_6 \rightarrow {}^5I_8$ of Ho^{3+} in $\text{NaYF}_4:2\%\text{Ho},20\%\text{Yb}@NaYF_4:40\%\text{Yb}$ NCs at different temperatures in the heating process in air. (c) Normalized UCL intensities of $\text{NaYF}_4:2\%\text{Ho},20\%\text{Yb}@NaYF_4:40\%\text{Yb}$ NCs in the vacuuming–filling cycle with filling different moist air upon 980 nm excitation at room temperature. (d) Luminescence decay curves of ${}^5I_6 \rightarrow {}^5I_8$ of Ho^{3+} in $\text{NaYF}_4:2\%\text{Ho},20\%\text{Yb}@NaYF_4:40\%\text{Yb}$ NCs measured in air and vacuum at room temperature.

vacuum. Interestingly, during the subsequent cooling process, the enhanced luminescence gradually decreases in air but continuously increases in vacuum.

The intensity variations of the green emission, Yb^{3+} emission, and ${}^5I_6 \rightarrow {}^5I_8$ emission with temperature changes in heating–cooling processes in air and in vacuum are depicted in Figure 2b and 2d, respectively. It can be seen from Figure 2d that the intensities of three emissions will be enhanced as soon as the vacuum is pumped at 300 K. This observation should be attributed to quenchers' desorption rather than laser-induced sample heating enhanced under vacuum conditions.^{41–44} On the one hand, the excitation power density used in the experiment is low enough that there should be no obvious thermal effect (it is about 2 orders of magnitude smaller than the lowest excitation power density reported in the literature). On the other hand, the thermal effect caused by laser-induced heating should be a relatively slow process, while the observed luminescence enhancement almost takes place with vacuum pumping at once. More experimental phenomena shown in Figure 2b,d indicating that the LTE is governed by quencher desorption will be discussed as follows. The decrease of luminescence intensity on cooling in air is attributed to readsorption of quenchers that exist in air. The enhancement of luminescence on cooling in vacuum is the consequence of no quenchers for readsorption in vacuum and suppression of multiphonon relaxation (MPR) with cooling. However, during the vacuum cooling process, unexpected luminescence quenching of Ho^{3+} can be seen from about 350 to 300 K. This phenomenon can be attributed to a heat-dependent energy transfer path: ${}^2F_{5/2}(\text{Yb}^{3+}) + {}^5I_8(\text{Ho}^{3+}) \rightarrow {}^2F_{7/2}(\text{Yb}^{3+}) + {}^5I_5(\text{Ho}^{3+})$. This energy transfer process needs to absorb a phonon, so it is more sensitive to temperature. When the temperature is lower than 350 K, it may lead to the deactivation of the energy transfer path from Yb^{3+} , thus resulting in luminescence quenching of Ho^{3+} during the

vacuum cooling process. When the vacuum-cooled sample is heated in vacuum again, the UCL intensities increase first and then decrease with the increase of temperature, which is basically reversible with the intensity–temperature curve in the first vacuum cooling process (Figure S3). It is also observed that at the same temperature, the amplitude of LTE in vacuum is higher than that in air because a negative pressure environment can promote quencher desorption. The luminescence intensity on heating in air reaches the maximum at 450 K, where the adsorbed quenchers on the surface of NCs should be depleted. The vacuum-induced enhancement of quencher desorption enables the depletion of the adsorbed quenchers at a lower temperature of 400 K, as shown in Figure 2d. The decrease of luminescence intensity at temperatures higher than 400 K on heating is attributed to the enhancement of MPR.⁴⁵ As a result, the heating–cooling experiments in air and in vacuum offer a conclusive evidence for quencher-desorption-induced LTE in $\text{NaYF}_4:2\%\text{Ho},20\%\text{Yb}@NaYF_4:40\%\text{Yb}$ NCs under 980 nm LD excitation. Furthermore, compared with heating in air, vacuum-assisted LTE has a higher amplification of LTE and ensure the repeatability of UCNCs. It can be seen from Figure 2 that the amplitude of green upconversion LTE at 400 K in vacuum is 3.7-fold, while that in air is only 2.6-fold. Even though the thermally enhanced intensity of UCL can continue increasing with the increase of temperature, too high a temperature will aggravate the quenching process caused by MPR and cause irreversible thermal damage of UCNCs.²² One of the thermal damage modes in fluoride UCNCs is caused by reaction with O_2 in air and forming oxy-fluoride. Hence, the vacuum-assisted LTE not only has low operating temperature to reduce the temperature-dependent quenching (MPR) and thermal damage but also provides a vacuum environment to protect UCNCs.

To further explore the process of the thermally enhanced green UCL in air, the temperature-dependent energy-level

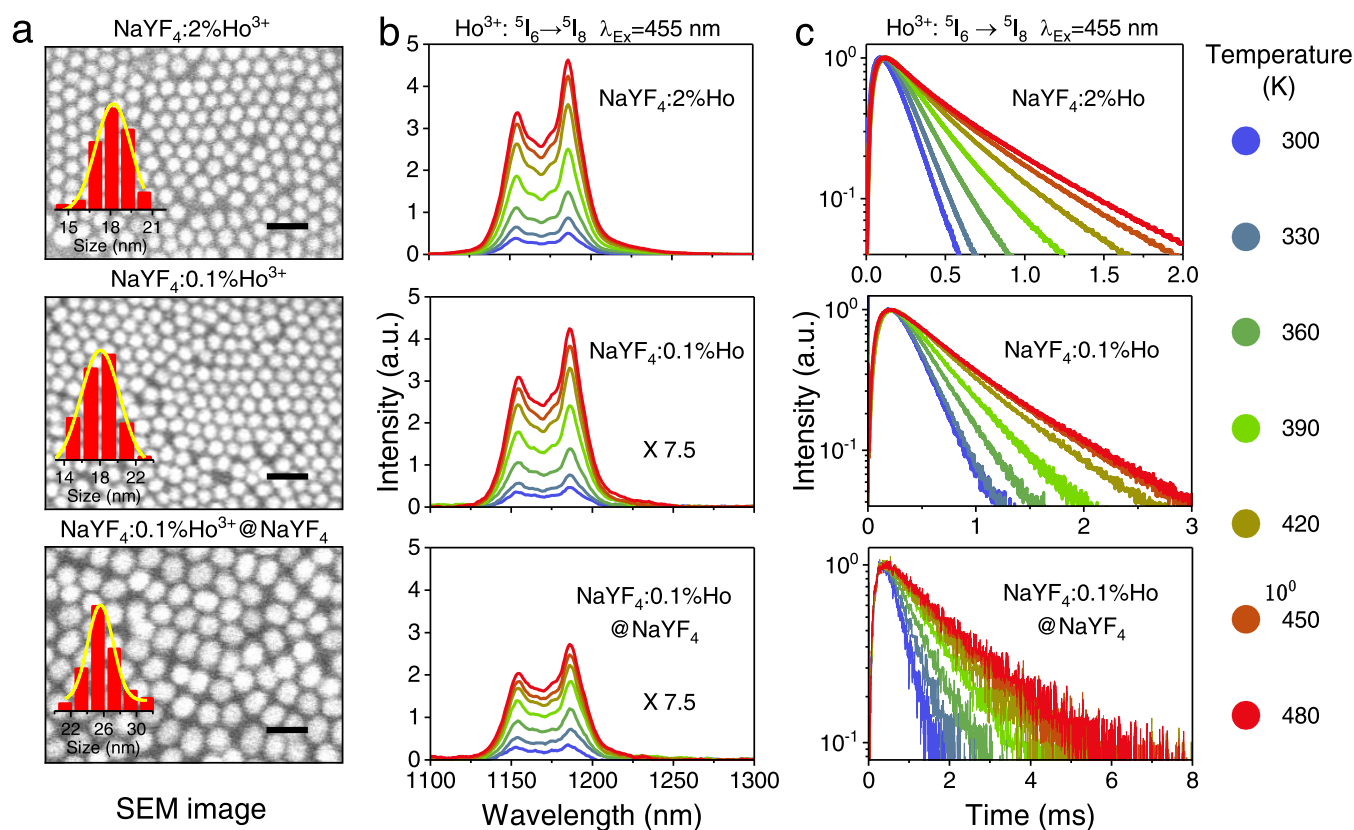


Figure 4. Demonstrating the long-range interaction between doped Ho³⁺ and adsorbed H₂O molecules in a series of Ho³⁺ singly doped NaYF₄ NCs. (a) SEM images, (b) temperature-dependent emission spectra, and (c) temperature-dependent luminescence decay curves of ⁵I₆ → ⁵I₈ in NaYF₄:2%Ho (top), NaYF₄:0.1%Ho (middle), and NaYF₄:0.1%Ho@NaYF₄ (bottom) NCs with elevated temperatures, under 455 nm LD excitation.

lifetimes of the ²F_{5/2} of Yb³⁺ and the ⁵I₆ of Ho³⁺ in the heating process are studied. It can be seen that the thermal enhancements of Yb³⁺ ²F_{5/2} → ²F_{7/2} emission and Ho³⁺ ⁵I₆ → ⁵I₈ emission (see Figure 2b) are accompanied by the remarkably prolonged emission lifetimes (Figure 3a,b), which indicates that the thermal-induced desorption of quenchers can alleviate the nonradiative process of both the ²F_{5/2} level of Yb³⁺ and the ⁵I₆ level of Ho³⁺. Since the ⁵I₆ level of Ho³⁺ is populated by energy transfer from the ²F_{5/2} level of Yb³⁺, the amount of transferred energy from Yb³⁺ to Ho³⁺ should increase in proportion to the increase of population of the Yb³⁺ ²F_{5/2} level on heating. However, the amplitude of LTE of the Ho³⁺ ⁵I₆ → ⁵I₈ emission is significantly larger than that of the Yb³⁺ ²F_{5/2} → ²F_{7/2} emission due to the thermally diminished nonradiative process of the ⁵I₆ level (meaning increased emission efficiency).

Experimental operation of vacuum pumping and moist air-filling cycles for regulating UCL intensity was conducted at room temperature. As shown in Figure 3c, the intensities of the green and red upconversion emissions are sensitive to vacuum and moist air-filling. Specifically, the upconversion emissions enhance in vacuum and reduce in moist air, which indicates that water molecules in the air are the adsorbent that causes luminescence quenching. It is also observed that the ⁵I₆ lifetime is prolonged in vacuum, as shown in Figure 3d. Owing to the fact that Ho³⁺ ions are located in the core of the core-shell NCs, the observed increase of thermal and vacuum-induced ⁵I₆ lifetimes (Figure 3b,d) suggests a long-range (shell

thickness) interaction between the interior Ho³⁺ and surface water molecules in the core-shell NCs.

To study the interaction between Ho³⁺ and adsorbed water molecules, we synthesized Ho³⁺ singly doped NaYF₄ NCs, i.e., NaYF₄:2%Ho, NaYF₄:0.1%Ho, and NaYF₄:0.1%Ho@NaYF₄, as seen in their SEM images in Figure 4a. The LTE of the ⁵I₆ → ⁵I₈ emission of Ho³⁺ singly doped samples under 455 nm excitation is observed with rising temperatures from 300 to 480 K, as shown in Figure 4b. One can find that the LTE of ⁵I₆ → ⁵I₈ emission is independent of the concentration of doped Ho³⁺; e.g., NaYF₄ NCs doped with 2%Ho³⁺ and 0.1%Ho³⁺ show almost the same LTE (see Figure 4b top and middle), which means that the interaction between Ho³⁺ and adsorbed water molecules remains almost unaffected by energy migration between Ho³⁺. After coating with an about 4 nm-thick inert shell (Figure 4a bottom), NaYF₄:0.1%Ho@NaYF₄ NCs still show a significant LTE of ⁵I₆ → ⁵I₈ emission (Figure 4b bottom). Furthermore, the extensions of ⁵I₆ state lifetimes of three samples with rising temperatures, as shown in Figure 4c, indicate that the origin of LTE for Ho³⁺ singly doped NaYF₄ NCs is the thermal-induced suppression of nonradiative deexcitation of the ⁵I₆ state. Hence, these pieces of evidence show that the interaction between Ho³⁺ and the adsorbed water molecule is a long-range interaction. However, LTE of Ho³⁺ caused by the long-range interaction is suppressed if the range is too long, e.g., Ho³⁺ singly doped NaYF₄ bulk materials show no LTE and thermal-induced increase of lifetime (see Figure S4).

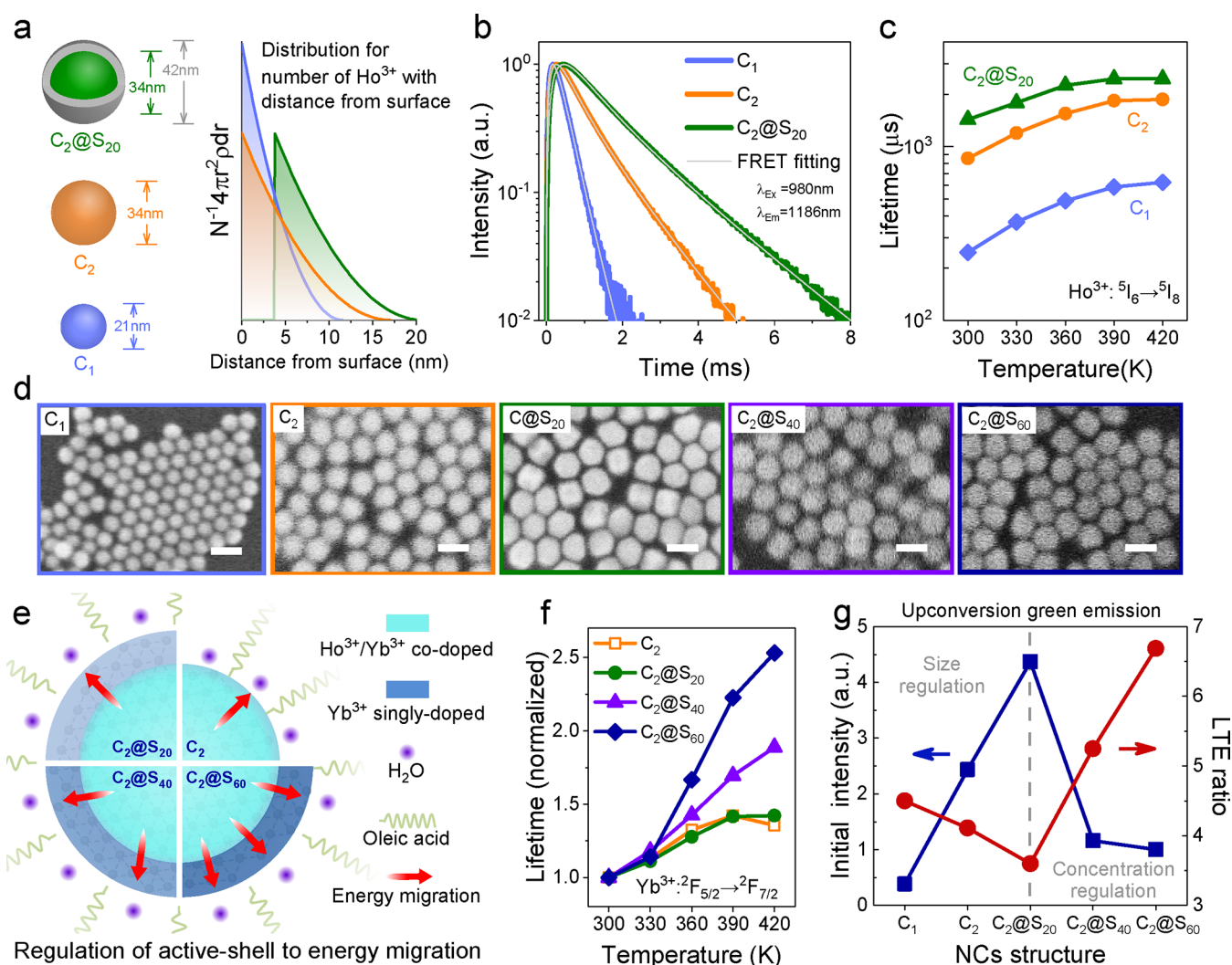


Figure 5. Regulation of LTE in $\text{Ho}^{3+}/\text{Yb}^{3+}$ doped NaYF_4 NCs using the different enhancement pathway of Ho^{3+} and Yb^{3+} . (a) Schematic diagram of distribution of the average number of Ho^{3+} with distance from the surface of NCs, according to the average number of Ho^{3+} in the spherical shell of $r \sim r + dr$ expressed as $4\pi r^2 \rho(r) dr$ (where r is the radius of the spherical shell, $\rho(r)$ is the density of doping Ho^{3+} , and N is the total number of Ho^{3+} in an NC). (b) Luminescence decay curves of the 5I_6 level and their fitting curves according to the FRET effect for C_1 , C_2 , and $C_2@S_{20}$ UCNCs. (c) Evolution of the luminescence lifetime of the 5I_6 level for C_1 , C_2 , and $C_2@S_{20}$ UCNCs under elevated temperatures. (d) SEM images of C_1 , C_2 , and a series of $C_2@S_x$ ($x = 20, 40, \text{ and } 60$) UCNCs. Scale bar is 50 nm. (e) Schematic illustration of the modulation of the energy migration rate from the interior to the surface of NCs by changing x in $C_2@S_x$ UCNCs. (f) Evolution of the luminescence decay lifetime values of the $^2F_{5/2}$ level in the thermal field of elevated temperatures for C_1 and $C_2@S_x$ ($x = 20, 40, \text{ and } 60$) UCNCs. (g) UCL intensity (blue line) at 300 K and the thermal enhancement ratio (red line) at 420 K for C_1 , C_2 , and $C_2@S_x$ ($x = 20, 40, \text{ and } 60$) UCNCs.

The long-range interaction of Ho^{3+} and adsorbed water molecules is inferred to as Förster resonance energy transfer (FRET) from the electron transition of $^5I_6 \rightarrow ^5I_7$ to the vibrational level of hydroxyl groups ($-\text{OH}$) because the high matching of energy between the two dipoles and the sufficient oscillator strength of $-\text{OH}$ provide support for long-range resonance.^{46–48} Furthermore, the temperature-dependent spectral measurement also supports this inference. Specifically, in the $\text{Ho}^{3+}/\text{Yb}^{3+}$ ETU system, if the 5I_7 level is only populated from the 5I_6 level through the MPR process, the LTE amplitude of the $^5I_7 \rightarrow ^5I_8$ emission should be slightly larger than that of the $^5I_6 \rightarrow ^5I_8$ emission in heating due to the thermally enhanced MPR process. However, the LTE amplitude of $^5I_7 \rightarrow ^5I_8$ is much smaller than that of $^5I_6 \rightarrow ^5I_8$ during the heating process (Figure S2). It indicates that there is an additional temperature-dependent nonradiative population path from the 5I_6 state to the 5I_7 state in addition to MPR,

which is probably the FRET effect between doped Ho^{3+} and adsorbed water molecules.

The pathway of interaction between Yb^{3+} and adsorbed water molecules was studied in a series of Yb^{3+} singly doped NaYF_4 NCs (the SEM images are shown in Figure S5). As shown in Figure S6, the emission intensity of Yb^{3+} in $\text{NaYF}_4:0.1\% \text{Yb}$ NCs shows slight thermal quenching. Meanwhile, it also can be seen from the temperature-dependent luminescence lifetime measurement that the depopulation rate of $^2F_{5/2}$ remains almost constant on heating (Figure S7). On comparing these results with temperature-dependent spectra of $\text{NaYF}_4:0.1\% \text{Yb}$ bulk materials (Figures S6 and S7), it can be concluded that doped Yb^{3+} and adsorbed water molecules have no long-range interactions. Moreover, once the concentration of Yb^{3+} is high enough for the excitation energy to migrate between doped Yb^{3+} , the LTE amplitude of $^2F_{5/2}$ in Yb^{3+} singly doped NaYF_4 NCs exhibits a strong concentration depend-

ence. For example, the LTE amplitude of ${}^2F_{5/2}$ for synthesized $\text{NaYF}_4:m\% \text{Yb}^{3+}$ ($m = 10, 20, 100$) NCs significantly increases with the increase of m (Figures S6 and S7). These results suggest that the energy transfer from Yb^{3+} to adsorbed water molecules only occurs on the surface (no long-range ET) of NCs, and the quenching of Yb^{3+} is realized through outward energy migration. This is why thermally enhanced luminescence of Yb^{3+} strongly depends on the doped concentration of Yb^{3+} .

These microscopic mechanisms of interaction between doped rare earth ions and adsorbed water molecules provide a new insight into the regulation of desorption-induced LTE. It is noteworthy that for the $\text{Ho}^{3+}/\text{Yb}^{3+}$ ETU system, the long-range interaction between Ho^{3+} and adsorbed water molecules causes the LTE of NCs to be size-dependent (determining the average distance between Ho^{3+} and adsorbed H_2O), while the surface quenching dependent on energy migration between Yb^{3+} leads to LTE of NCs to be Yb^{3+} -concentration-dependent. Hence, based on the different LTE properties of Ho^{3+} and Yb^{3+} , we discuss the regulation of LTE according to the size of NCs and the doping concentration of Yb^{3+} .

Based on previous discussions, the interaction between Ho^{3+} and adsorbed H_2O on the surface is strongly distance-dependent. Three kinds of UCNCs with different sizes or core-shell structures (SEM images in Figure 5d), i.e., 21 nm bare core $\text{NaYF}_4:2\% \text{Ho}20\% \text{Yb}$ NCs (C_1), 34 nm bare core $\text{NaYF}_4:2\% \text{Ho}20\% \text{Yb}$ NCs (C_2), and 42 nm core-shell $\text{NaYF}_4:2\% \text{Ho}20\% \text{Yb}@ \text{NaYF}_4:20\% \text{Yb}$ NCs ($C_2@S_{20}$), were synthesized to regulate the interaction between Ho^{3+} and adsorbed water molecules. The spatial distributions of doped Ho^{3+} in three designed nanomaterials are simulated in Figure 5a. It can be seen that increasing the size of NCs or the coating shell can reduce the distribution of Ho^{3+} near the surface of NCs. These modulation methods make doped Ho^{3+} in the samples have different degrees of interaction with adsorbed water molecules, which can be verified by measuring the luminescence decay of the 5I_6 state. As shown in Figure 5b, the luminescence decay curves of three samples show that they have obviously different lifetimes of the 5I_6 state and follow an ordering rule that the more doped Ho^{3+} are distributed near the surface of NCs, the shorter the lifetime of the 5I_6 state. In addition, to further confirm the causal relationship between the spatial distribution of Ho^{3+} and the luminescence lifetime of the 5I_6 state, the fitting curves of luminescence decay are built according to the FRET effect and are well consistent with the luminescence decay curves of the ${}^5I_6 \rightarrow {}^5I_8$ emission (gray lines in Figure 5b), which determines the decisive role of the spatial distribution of Ho^{3+} on the luminescence lifetime of the 5I_6 state (see Figure S8 for more fitting details).³⁷ Hence, the large value of 5I_6 lifetimes estimated from the luminescence decay curve implies the low degree of interaction between Ho^{3+} and adsorbed water molecules. Moreover, one can see from Figure 5c that the sample with a short 5I_6 lifetime shows a large thermal enhancement amplitude in the heating process, which verifies the correctness of the previous inference and also indicates that the strategy of modulating spatial distributions of Ho^{3+} successfully regulates the LTE properties of Ho^{3+} .

Considering that the degree of interaction between Yb^{3+} and adsorbed water molecules is dependent on the doped concentration of Yb^{3+} , according to a previous discussion, a series of active-core/active-shell structural UCNCs of $\text{NaYF}_4:2\% \text{Ho}, 20\% \text{Yb}@ \text{NaYF}_4:x\% \text{Yb}$ (namely, $C_2@S_x$, $x = 40$ and 60; SEM images are shown in Figure 5d) with different

doping concentrations of Yb^{3+} in the active shell were synthesized. The design intent of active-shell coating NCs, as schematically shown in Figure 5e, is that changing x can not only control the energy migration rate without influencing the environment around the activator as much as possible but also affect the surface quenching rate of Yb^{3+} , both of which can promote or inhibit the energy transfer rate from Yb^{3+} to adsorbed water molecules. The thermally enhanced amplitudes of luminescence lifetime of $\text{Yb}^{3+} {}^2F_{5/2}$ for C_2 and $C_2@S_x$ samples ($x = 20, 40$, and 60), as expected, increase with the increase of x (as shown in Figure 5f). It is also worth noting that the thermally enhanced trends for C_2 and $C_2@S_{20}$ NCs are almost identical (orange and green lines in Figure 5f), meaning that the influence of the surface Yb^{3+} concentration on LTE of Yb^{3+} is much greater than that of the size of NCs. These results indicate that the adjustment of the Yb^{3+} concentration located on the surface of NC can effectively regulate the thermally enhanced luminescent behavior of Yb^{3+} doped UCNCs.

The results of regulating upconversion LTE (green emission) by adjusting the size and doping concentration of UCNCs are shown in Figure 5g. It can be seen that decreasing the size of NCs and increasing the concentration of doping Yb^{3+} in the active shell can both significantly enhance the amplitude of upconversion LTE (red line). Specifically, the $C_2@S_{20}$ sample has the smallest upconversion LTE amplitude of about 3.5-fold (see Figure S9 for more analysis). The smaller size core UCNCs of C_1 have a 4.5-fold amplitude of upconversion LTE, while the $C_2@S_{60}$ sample has the largest upconversion LTE amplitude of about 6.7-fold. In other words, under the premise of limited size reduction of UCNCs, increasing the Yb^{3+} concentration doped in the active shell can bring a higher amplitude of upconversion LTE. Furthermore, one may also find that the UCL intensity at room temperature (blue line) and the thermal enhancement ratio at high temperature (red line) have the opposite trend. This may be a disappointing phenomenon, which means that the increasing amplitude of upconversion LTE obtained by modulating the size or concentration of UCNCs is at the cost of reducing the UCL intensity. However, since this phenomenon promotes the contrast between samples, it can have a better application in the field of anticounterfeiting.

CONCLUSIONS

The vacuum spectral experiment in this work provides conclusive evidence for the mechanism of LTE that the temperature-dependent desorption of adsorbed water molecules alleviates luminescence quenching in $\text{Ho}^{3+}/\text{Yb}^{3+}$ doped NaYF_4 UCNCs. With the cooperation of vacuuming and heating, a stronger enhancement of UCL can be obtained. Furthermore, a strong long-range FRET effect between the ${}^5I_6 \rightarrow {}^5I_7$ transition of Ho^{3+} and the $-\text{OH}$ vibration of surface-adsorbed water is found, which means that Ho^{3+} , as the activator, also has a great contribution to the LTE of NCs. According to the different deexcitation pathways of $\text{Ho}^{3+}/\text{Yb}^{3+}$, which, respectively, depend on the average distance from the adsorbed H_2O and the doping concentration, the amplitude of upconversion LTE of $\text{Ho}^{3+}/\text{Yb}^{3+}$ codoped NaYF_4 NCs is successfully regulated from 3.5-fold to 6.7-fold by varying the size of NCs and coating the active shell with different doping concentrations of Yb^{3+} while maintaining the NC size relatively large (>30 nm). These findings provide a methodological reference and theoretical support for the regulation of the thermal enhancement of UCL in various applications.

■ ASSOCIATED CONTENT

SI Supporting Information

The Supporting Information is available free of charge at <https://pubs.acs.org/doi/10.1021/acssuschemeng.2c05408>.

Schematic diagram of the vacuum spectrum experimental device; more spectral data (emission spectrum and luminescence decay) with different temperatures in air or vacuum for the samples mentioned in the report; SEM images of some samples mentioned in the report; fitting details of luminescence decay curves; and discussion on the regulation result of UCLTE through coating the active shell (PDF)

■ AUTHOR INFORMATION

Corresponding Authors

Feng Liu – Key Laboratory for UV-Emitting Materials and Technology of Ministry of Education, Northeast Normal University, Changchun 130024, China; orcid.org/0000-0002-7310-8763; Email: fengliu@nenu.edu.cn

Jiahua Zhang – State Key Laboratory of Luminescence and Applications, Changchun Institute of Optics, Fine Mechanics and Physics, Chinese Academy of Sciences, Changchun 130033, China; Center of Materials Science and Optoelectronic Engineering, University of Chinese Academy of Sciences, Beijing 100049, China; orcid.org/0000-0001-5180-7267; Email: zhangjh@ciomp.ac.cn

Authors

Lin Yang – State Key Laboratory of Luminescence and Applications, Changchun Institute of Optics, Fine Mechanics and Physics, Chinese Academy of Sciences, Changchun 130033, China; Center of Materials Science and Optoelectronic Engineering, University of Chinese Academy of Sciences, Beijing 100049, China; orcid.org/0000-0002-2140-2039

Hao Wu – State Key Laboratory of Luminescence and Applications, Changchun Institute of Optics, Fine Mechanics and Physics, Chinese Academy of Sciences, Changchun 130033, China; orcid.org/0000-0002-8396-7393

Guo-hui Pan – State Key Laboratory of Luminescence and Applications, Changchun Institute of Optics, Fine Mechanics and Physics, Chinese Academy of Sciences, Changchun 130033, China; orcid.org/0000-0002-2190-2690

Liangliang Zhang – State Key Laboratory of Luminescence and Applications, Changchun Institute of Optics, Fine Mechanics and Physics, Chinese Academy of Sciences, Changchun 130033, China; orcid.org/0000-0002-9546-8786

Huajun Wu – State Key Laboratory of Luminescence and Applications, Changchun Institute of Optics, Fine Mechanics and Physics, Chinese Academy of Sciences, Changchun 130033, China

Zhendong Hao – State Key Laboratory of Luminescence and Applications, Changchun Institute of Optics, Fine Mechanics and Physics, Chinese Academy of Sciences, Changchun 130033, China

Complete contact information is available at: <https://pubs.acs.org/doi/10.1021/acssuschemeng.2c05408>

Notes

The authors declare no competing financial interest.

■ ACKNOWLEDGMENTS

This work was partially supported by the National Natural Science Foundation of China (Grant Nos. 11874055, 11904361, and 52072361), the Youth Innovation Promotion Association CAS No. 2020222, Key Research and Development Program of Jilin province (20200401050GX, 20200401004GX, and 20210201024GX), and the Opening Project Key Laboratory of Transparent Opto-functional Inorganic Material, Chinese Academy of Sciences.

■ REFERENCES

- (1) Chen, X.; Peng, D.; Ju, Q.; Wang, F. Photon Upconversion in Core–Shell Nanoparticles. *Chem. Soc. Rev.* **2015**, *44*, 1318–1330.
- (2) Deng, R.; Qin, F.; Chen, R.; Huang, W.; Hong, M.; Liu, X. Temporal Full-Colour Tuning through Non-Steady-State Upconversion. *Nat. Nanotechnol.* **2015**, *10*, 237.
- (3) Du, K.; Feng, J.; Gao, X.; Zhang, H. Nanocomposites Based on Lanthanide-Doped Upconversion Nanoparticles: Diverse Designs and Applications. *Light: Sci. Appl.* **2022**, *11*, No. 222.
- (4) Fernandez-Bravo, A.; Wang, D. Q.; Barnard, E. S.; Teitelboim, A.; Tajon, C.; Guan, J.; Schatz, G. C.; Cohen, B. E.; Chan, E. M.; Schuck, P. J.; Odom, T. W. Ultralow-Threshold, Continuous-Wave Upconverting Lasing from Subwavelength Plasmons. *Nat. Mater.* **2019**, *18*, 1172–1176.
- (5) Luo, Y.; Liu, Y.; Wang, C.; Bai, G.; Shen, Y.; Jiang, Z.; Xu, S.; Chen, L. Near-Infrared Anti-Stokes Luminescence from Neodymium Doped Perovskite Calcium Titanate Particles for Optical Temperature Sensors. *Sens. Actuators, A* **2021**, *326*, No. 112741.
- (6) Wang, F.; Wen, S.; He, H.; Wang, B.; Zhou, Z.; Shimoni, O.; Jin, D. Microscopic Inspection and Tracking of Single Upconversion Nanoparticles in Living Cells. *Light: Sci. Appl.* **2018**, *7*, 18007.
- (7) Tian, Q.; Yao, W.; Wu, W.; Liu, J.; Wu, Z.; Liu, L.; Dai, Z.; Jiang, C. An Efficient UV-Vis-NIR Responsive Upconversion and Plasmonic Enhanced Photocatalyst Based on Lanthanide-Doped NaYF₄/SnO₂/Ag. *ACS Sustainable Chem. Eng.* **2017**, *5*, 10889–10899.
- (8) Gnanasammandhan, M. K.; Idris, N. M.; Bansal, A.; Huang, K.; Zhang, Y. Near-IR Photoactivation Using Mesoporous Silica-Coated NaYF₄:Yb,Er/Tm Upconversion Nanoparticles. *Nat. Protoc.* **2016**, *11*, 688–713.
- (9) Xu, X.; Li, W.; Hu, C.; Lei, B.; Zhang, X.; Li, Y.; Zhan, Q.; LiU, Y.; Zhuang, J. Promoting the Growth of Mung Bean Plants through Uptake and Light Conversion of NaYF₄:Yb,Er@CDs Nanocomposites. *ACS Sustainable Chem. Eng.* **2020**, *8*, 9751–9762.
- (10) Li, D.; Shao, Q.; Dong, Y.; Jiang, J. Anomalous Temperature-Dependent Upconversion Luminescence of Small-Sized NaYF₄:Yb³⁺, Er³⁺ Nanoparticles. *J. Phys. Chem. C* **2014**, *118*, 22807–22813.
- (11) Mi, C.; Zhou, J.; Wang, F.; Lin, G.; Jin, D. Ultrasensitive Ratiometric Nanothermometer with Large Dynamic Range and Photostability. *Chem. Mater.* **2019**, *31*, 9480–9487.
- (12) Hu, Y.; Shao, Q.; Deng, X.; Song, D.; Han, S.; Dong, Y.; Jiang, J. Thermally Induced Multicolor Emissions of Upconversion Hybrids with Large Color Shifts for Anticounterfeiting Applications. *J. Mater. Chem. C* **2019**, *7*, 11770.
- (13) Lei, L.; Xia, J.; Chen, Y.; Wang, Y.; Bai, G.; Xia, H.; Xu, S. Enhancing Negative Thermal Quenching Effect Via Low-Valence Doping in Two-Dimensional Confined Core-Shell Upconversion Nanocrystals. *J. Mater. Chem. C* **2018**, *6*, 11587.
- (14) Shao, Q.; Zhang, G.; Ouyang, L.; Hu, Y.; Dong, Y.; Jiang, J. Emission Color Tuning of Core/Shell Upconversion Nanoparticles through Modulation of Laser Power or Temperature. *Nanoscale* **2017**, *9*, 12132.
- (15) Wang, Y.; Lei, L.; Ye, R.; Jia, G.; Hua, Y.; Deng, D.; Xu, S. Integrating Positive and Negative Thermal Quenching Effect for Ultrasensitive Ratiometric Temperature Sensing and Anti-Counterfeiting. *ACS Appl. Mater. Interfaces* **2021**, *13*, 23951–23959.

- (16) Shi, R.; Martinez, E. D.; Brites, C. D. S.; Carlos, L. D. Thermal Enhancement of Upconversion Emission in Nanocrystals: A Comprehensive Summary. *Phys. Chem. Chem. Phys.* **2021**, *23*, 20.
- (17) Zhou, Y.; Cheng, Y.; Huang, Q.; Xu, J.; Lin, H.; Wang, Y. Abnormal Thermally Enhanced Upconversion Luminescence of Lanthanide-Doped Phosphors: Proposed Mechanisms and Potential Applications. *J. Mater. Chem. C* **2021**, *9*, 2220.
- (18) Wang, Y.; Chen, B.; Wang, F. Overcoming Thermal Quenching in Upconversion Nanoparticles. *Nanoscale* **2021**, *13*, 3454.
- (19) Zhou, J.; Wen, S.; Liao, J.; Clarke, C.; Tawfik, S. A.; Ren, W.; Mi, C.; Wang, F.; Jin, D. Activation of the Surface Dark-Layer to Enhance Upconversion in a Thermal Field. *Nat. Photonics* **2018**, *12*, 154–158.
- (20) Mi, C.; Zhou, J.; Wang, F.; Jin, D. Thermally Enhanced NIR-NIR Anti-Stokes Emission in Rare Earth Doped Nanocrystals. *Nanoscale* **2019**, *11*, 12547–12552.
- (21) Wang, Z.; Christiansen, J.; Wezendonk, D.; Xie, X.; Huis, M. A. v.; Meijerink, A. Thermal Enhancement and Quenching of Upconversion Emission in Nanocrystals. *Nanoscale* **2019**, *11*, 12188–12197.
- (22) Li, D.; Wang, W.; Liu, X.; Jiang, C.; Qiu, J. Discovery of Non-Reversible Thermally Enhanced Upconversion Luminescence Behavior in Rare-Earth Doped Nanoparticles. *J. Mater. Chem. C* **2019**, *7*, 4336.
- (23) Martínez, E. D.; García-Flores, A.; Carneiro Neto, A.; Brites, C.; Carlos, L.; Urbano, R.; Rettori, C. Controlling the Thermal Switching in Upconverting Nanoparticles through Surface Chemistry. *Nanoscale* **2021**, *13*, 16267.
- (24) Hu, Y.; Shao, Q.; Zhang, P.; Dong, Y.; Fang, F.; Jiang, J. Mechanistic Investigations on the Dramatic Thermally-Induced Luminescence Enhancement in Upconversion Nanocrystals. *J. Phys. Chem. C* **2018**, *122*, 26142–26152.
- (25) Cui, X.; Yao, C.; Hang, L.; Feng, H.; Wu, Q.; Wang, Y. Size-Dependent Abnormal Thermo-Enhanced Luminescence of Ytterbium-Doped Nanoparticles. *Nanoscale* **2017**, *9*, 13794–13799.
- (26) Zhou, Y.; Cheng, Y.; Xu, J.; Lin, H.; Wang, Y. Thermo-Enhanced Upconversion Luminescence in Inert-Core/Active-Shell Ucnps: The Inert Core Matters. *Nanoscale* **2021**, *13*, 6569.
- (27) Dąbrowski, A. Adsorption-from Theory to Practice. *Adv. Colloid Interface Sci.* **2001**, *93*, 135–224.
- (28) Arppe, R.; Hyppnen, I.; Perl, N.; Peltomaa, R.; Kaiser, M.; Würth, C.; Christ, S.; Resch-Genger, U.; Schferling, M.; Soukka, T. Quenching of the Upconversion Luminescence of NaYF₄:Yb,Er and NaYF₄:Yb,Tm Nanophosphors by Water: The Role of the Sensitizer Yb in Non-Radiative Relaxation. *Nanoscale* **2015**, *7*, 11746.
- (29) Hossan, M. Y.; Hor, A.; Luu, Q. A.; Smith, S. J.; Ma, P. S.; Berry, M. T. Explaining the Nanoscale Effect in the Upconversion Dynamics of β -NaYF₄:Yb³⁺, Er³⁺ Core and Core-Shell Nanocrystals. *J. Phys. Chem. C* **2017**, *121*, 16592–16606.
- (30) Mei, S.; Zhou, J.; Sun, H.; Cai, Y.; Sun, L.; Jin, D.; Yan, C. Networking State of Ytterbium Ions Probing the Origin of Luminescence Quenching and Activation in Nanocrystals. *Adv. Sci.* **2021**, *8*, No. 2003325.
- (31) Chen, B.; Kong, W.; Wang, N.; Zhu, G.; Wang, F. Oleylamine-Mediated Synthesis of Small NaYbF₄ Nanoparticles with Tunable Size. *Chem. Mater.* **2019**, *31*, 4779–4786.
- (32) Fischer, S.; Bronstein, N. D.; Swabeck, J. K.; Chan, E. M.; Alivisatos, A. P. Precise Tuning of Surface Quenching for Luminescence Enhancement in Core-Shell Lanthanide-Doped Nanocrystals. *Nano Lett.* **2016**, *16*, 7241–7247.
- (33) Labrador-Páez, L.; Kostiv, U.; Widengren, J.; Liu, H. Water: An Influential Agent for Lanthanide-Doped Luminescent Nanoparticles in Nanomedicine. *Adv. Opt. Mater.* **2022**, No. 2200513.
- (34) Johnson, N. J. J.; He, S.; Diao, S.; Chan, E. M.; Dai, H.; Almutairi, A. Direct Evidence for Coupled Surface and Concentration Quenching Dynamics in Lanthanide-Doped Nanocrystals. *J. Am. Chem. Soc.* **2017**, *139*, 3275–3282.
- (35) Wang, F.; Wang, J.; Liu, X. Direct Evidence of a Surface Quenching Effect on Size-Dependent Luminescence of Upconversion Nanoparticles. *Angew. Chem., Int. Ed.* **2010**, *49*, 7456–7460.
- (36) Hu, Y.; Shao, Q.; Dong, Y.; Jiang, J. Energy Loss Mechanism of Upconversion Core/Shell Nanocrystals. *J. Phys. Chem. C* **2019**, *123*, 22674–22679.
- (37) Rabouw, F. T.; Prins, P. T.; Villanueva-Delgado, P.; Castelijns, M.; Geitenbeek, R. G.; Meijerink, A. Quenching Pathways in NaYF₄:Er³⁺,Yb³⁺ Upconversion Nanocrystals. *ACS Nano* **2018**, *12*, 4812–4823.
- (38) Guo, S.; Xie, X.; Huang, L.; Huang, W. Sensitive Water Probing through Nonlinear Photon Upconversion of Lanthanide-Doped Nanoparticles. *ACS Appl. Mater. Interfaces* **2016**, *8*, 847–853.
- (39) Qian, H.-S.; Zhang, Y. Synthesis of Hexagonal-Phase Core-Shell NaYF₄ Nanocrystals with Tunable Upconversion Fluorescence. *Langmuir* **2008**, *24*, 12123–12125.
- (40) Johnson, N. J. J.; Korinek, A.; Dong, C.; Veggel, F. Self-Focusing by Ostwald Ripening: A Strategy for Layer-by-Layer Epitaxial Growth on Upconverting Nanocrystals. *J. Am. Chem. Soc.* **2012**, *134*, 11068–11071.
- (41) Runowski, M.; Woz'ny, P.; Lis, S.; Lavín, V.; Martín, L. Optical Vacuum Sensor Based on Lanthanide Upconversion-Luminescence Thermometry as a Tool for Ultralow Pressure Sensing. *Adv. Mater. Technol.* **2020**, *5*, No. 1901091.
- (42) Soler-Carracedo, K.; Soler-Carracedo, K.; Martín, I.; Runowski, M.; Martín, L.; Martín, L. L.; Lahoz, F.; Lahoz, F.; Lozano-Gorrín, A.; Lozano-Gorrín, A. D.; Paz-Buclatin, F. Luminescent Nd³⁺-Based Microresonators Working as Optical Vacuum Sensors. *Adv. Opt. Mater.* **2020**, *8*, No. 2000678.
- (43) Silva Filho, C. I.; Oliveira, A.; Pereira, S.; Sá, G.; Luz, L.; Júnior, S. Bright Thermal (Blackbody) Emission of Visible Light from LnO² (Ln = Pr, Tb), Photoinduced by a NIR 980 nm Laser. *Dalton Trans.* **2019**, *48*, 2574–2581.
- (44) Runowski, M.; Woz'ny, P.; Martín, I. Optical Pressure Sensing in Vacuum and High-Pressure Ranges Using Lanthanide-Based Luminescent Thermometer–Manometer. *J. Mater. Chem. C* **2021**, *9*, 4643–4651.
- (45) Layne, C. B.; Lowdermilk, W. H.; Weber, M. Multiphonon Relaxation of Rare-Earth Ions in Oxide Glasses. *Phys. Rev. B* **1977**, *16*, 10–16.
- (46) Chen, T.; He, B.; Tao, J.; He, Y.; Zheng, Y.; et al. Application of Förster Resonance Energy Transfer (FRET) Technique to Elucidate Intracellular and in Vivo Biofate of Nanomedicines. *Adv. Drug Delivery Rev.* **2019**, *143*, 177–205.
- (47) Feng, Y.; Li, Z.; Li, Q.; Yuan, J.; Tu, L.; Ning, L.; Zhang, H. Internal OH⁻ Induced Cascade Quenching of Upconversion Luminescence in NaYF₄:Yb/Er Nanocrystals. *Light: Sci. Appl.* **2021**, *10*, 105.
- (48) Reimers, J. R.; Watts, R. O. Analysis of the OH Bend and Stretch Region in the Vibrational Spectrum of Water. *Chem. Phys. Lett.* **1983**, *94*, 222–226.